Plasma Chemistry and Plasma Processing (2022) 42:709–730
https://doi.org/10.1007/s11090-022-10253-3

ORIGINAL PAPER

Optimization of Non-thermal Plasma-Assisted Catalytic Oxidation for Methane Emissions Abatement as an Exhaust Aftertreatment Technology

Rahman Gholami[1] · Cristina Stere[1] · Sarayute Chansai[1] · Amit Singhania[1] · Alexandre Goguet[2] · Peter Hinde[3] · Paul Millington[3] · Christopher Hardacre[1]

Received: 4 January 2022 / Accepted: 18 April 2022 / Published online: 12 May 2022

Abstract
While methane-powered vehicles produce fewer greenhouse gas emissions in comparison to conventional fuel vehicles, there is a significant amount of methane slip in their exhaust that needs to be treated. This study investigates non-thermal plasma (NTP) assisted catalytic methane oxidation as an alternative method for the low temperature methane slip abatement applicable to the exhaust of biogas methane-powered vehicles. It is concluded that high CH_4 conversion and CO_2 selectivity can be obtained using NTP-catalysis at low temperature with Pd/Al_2O_3 found to be the most promising candidate among all catalysts tested. In addition, it was found that CH_4 conversion efficiency was dependent on the feed gas components and gas hourly space velocity as well as how the activation energy is introduced. For example, a combination of plasma and external heat supply provides advantages in terms of CH_4 conversion along with lower plasma energy consumption. The presence of N_2 and O_2 in the feed gas during NTP-catalytic methane oxidation results in unfavourable NO_X formation which linearly increases with CH_4 conversion. These results conclude that the most suitable aftertreatment option involves the combination of an oxidation catalyst with plasma to target the hydrocarbon and CH_4 oxidation, followed by an ammonia-SCR system to convert the NO_X formed in plasma assisted zone.

Keywords Methane oxidation · Pd/Al_2O_3 · Plasma DBD · NOx · NH_3-SCR · Exhaust gas cleaning

✉ Christopher Hardacre
c.hardacre@manchester.ac.uk

[1] Department of Chemical Engineering and Analytical Science, The University of Manchester, Manchester M13 9PL, UK

[2] School of Chemical Engineering and Chemistry, The Queen's University of Belfast, Belfast BT9 5AG, UK

[3] Johnson Matthey Technology Centre, Reading, UK

Introduction

Methane-powered vehicles have gained recent interest, with currently 23 million vehicles worldwide, due to their life cycle greenhouse gas (GHG) emissions benefits over conventional gasoline- and diesel- powered vehicles [1–3]. The use of methane as a fuel, either from fossil derived natural gas or renewable natural gas (biomethane), can reduce GHG emissions as well as other air pollutants. However, these benefits are mitigated by the presence of a significant amount of biogas derived-unburned methane (methane slip) in the engine exhaust [4], in particular during cold-start. Methane is a strong GHG with global warming potential which is 21 times higher than that of carbon dioxide. The low gas temperatures and the presence of impurities in the vehicle exhaust make the current catalytic converters inefficient for the methane removal and new and novel exhaust aftertreatment systems are required.

The thermal catalytic oxidation of methane has been extensively investigated [5–8]. However, even for the most active catalysts, 100% conversion cannot be achieved at temperatures below 400 °C, especially when water is present. An alternative approach to activate CH_4 at low temperatures is to utilize non-thermal plasma (NTP). Typically, gas phase NTP reactions are nonselective; however, combining an NTP with catalyst can improve the system performance in terms of conversion and product selectivity [9–11]. Most plasma-catalyst studies have used a dielectric barrier discharge (DBD) reactor [12–14] with one or more dielectric material and a catalyst that either filled the gap between the plasma electrodes or placed after the discharge zone. NTP-assisted catalytic systems, using different reactor configurations, have received a lot of attentions in the literature for various reactions including dry reforming of methane [15, 16], CO_2 hydrogenation [17, 18], NO_X reduction [19] and the water–gas shift reaction [20]. Although there are a number of studies that have examined the NTP-assisted catalytic methane oxidation, few have studied it under conditions relevant to methane-powered vehicles exhaust applications [21, 22].

One of the concerns with plasma-catalyst systems for the methane oxidation is the benefits brought by the hybridization of the plasma and the catalyst. For example, the synergistic effect between the plasma and the catalyst for this reaction depends on several factors including the nature of power supply [21] and the reaction conditions [21–23]. While some researchers questioned such synergy and attributed the catalytic effect mostly to the subsequent CO oxidation [22], others reported a true synergistic effect on the CH_4 conversion [23]. An *in-situ* study of the role of the NTP in the hybrid catalytic reaction under CH_4 and $CH_4 + O_2$ conditions has provided evidence that no significant structural changes occurred within the catalyst on application of the NTP and that the temperature of the Pd nanoparticles was lower than that necessary to activate the thermal CH_4 oxidation reaction [24]. Under similar conditions, using a diffuse reflectance infra-red Fourier transform spectroscopy coupled with mass spectrometer (DRIFTS-MS) cell, an enhancement in the formation of surface species on the Pd catalyst was reported [25]. Upon review of the body of work reported to date, the role of the catalyst during methane oxidation in the plasma-catalyst systems remains unclear. In addition, the effect of the components in a gas mixture that mimics the exhaust gas conditions, on the methane conversion and product selectivity needs to be clarified.

While the high endothermicity of the methane dissociation (434 kJ/mol) plays a crucial role in the plasma assisted reaction, the impact of high concentrations of H_2O, CO_2, O_2 and N_2/NO_X has not been explored in detail. Baylet et al. [22] showed that an understanding of the undesirable side reactions in the plasma-only system, the role of CO_2 and water in the

plasma assisted catalytic process needs to be clarified. Moreover, the presence of N_2 and O_2 in the feed gas during plasma-assisted methane oxidation has been reported to result in NO_X formation [22] and there are no reported investigation on the relationship between methane conversion and NO_X formation in complex feed gas mixtures with the plasma-catalyst systems. In terms of temperature dependence, an increase in the reactor temperature to 200 °C was shown to have a positive effect on the CH_4 conversion [22]. Nozaki et al. [26] discussed that the dissociation of methane by electron impact was almost independent of the reaction temperature and that the vibrationally excited methane and water were the activated species at low temperature. Considering that the range of temperature experienced by the exhaust gas is wide, e.g. up to 300 °C when considering cold start conditions, the effect of temperature should be examined in more detail.

Previously, the NTP-assisted catalytic methane oxidation has only been explored using Pd/Al_2O_3, Al_2O_3, Ru/TiO_2 and Au/Al_2O_3 [27–29]. In order to investigate how the type of catalyst affects the performance of the plasma-catalyst and identify the best catalyst formulation for this reacting system, several supported metal catalysts were prepared and tested under the same reaction conditions. The selected catalysts in this study were among the ones reported for CH_4 activation for a wide range of reactions [30–33]. The aim of this study is to investigate the effect of the nature of the catalyst, the feed gas components as well as operating temperature conditions on the plasma-catalyst system performance in the methane oxidation reaction. Herein, an investigation of NO_X production due to uncontrolled plasma reactions between N_2 and O_2 present in the gas stream and the link to methane conversion is established as well as strategies to mitigate NO_X slip.

Experimental and Methods

Catalyst Preparation

The catalysts were prepared by incipient wetness impregnation. A NH_4-ZSM-5 (Zeolyst International, molar SiO_2/Al_2O_3 ratio of 30 and 80, approximately 0.17 $cm^3\ g^{-1}$ pore volume) was calcined in air at 550 °C for 8 h to obtain the H-ZSM-5 form (denoted ZSM-5). γ-Al_2O_3 was obtained from Sasol which had a pore volume of 0.5 $cm^3\ g^{-1}$ and this was dried in ambient air at 110 °C for 8 h. Both the ZSM-5 and γ-Al_2O_3 powders were pressed into pellets before being ground and sieved between 250 and 425 µm mesh sizes particles. The ZSM-5 or γ-Al_2O_3 supports were impregnated with solutions made by dissolving an appropriate amount of $Co(NO_3)_2{\cdot}6H_2O$ (99.999%, Sigma-Aldrich), $Cu(NO_3)_2{\cdot}xH_2O$ (99.999%, Sigma-Aldrich), $Fe(NO_3)_3{\cdot}9H_2O$ (≥98%, Sigma-Aldrich), $LiNO_3$ (99.99%, Sigma-Aldrich), $(NH_4)_6Mo_7O_{24}{\cdot}4H_2O$ (99.98%, Sigma-Aldrich), $Ni(NO_3)_2{\cdot}6H_2O$ (99.999%, Sigma-Aldrich) or $Pd(NO_3)_2{\cdot}2H_2O$ (99%, Sigma-Aldrich) in 10 wt% HNO_3 (prepared from concentrated HNO_3 (69–70%, BDH)) or diluting an appropriate amount of ruthenium (III) nitrosyl nitrate solution (1.5 wt% Ru, $Ru(NO)(NO_3)_x(OH)_y$ $x+y=3$, Sigma-Aldrich) or rhodium (III) nitrate solution (10 wt% Rh, $Rh(NO_3)_3$, Sigma-Aldrich) in deionized water. After 48 h impregnation, the impregnated samples were dried in air at 110 °C for 8 h. The dried precursors were subsequently calcined in flowing air at 500 °C for 8 h following a temperature ramp of 10 °C min^{-1} and then, cooled to room temperature before testing. The alumina-based catalysts were prepared to obtain 2 wt% nominal loading of Ru, Co, Fe, Cu, Rh, Pt, Ni or Li and 10 wt% nominal loading of Pd. A 2 wt% Pd/Al_2O_3 was also tested and was obtained from Johnson Matthey.

Experimental Setup

A schematic representation of the experimental setup is shown in Fig. 1. It consisted of a quartz tubular reactor (outside diameter (O.D.): 6 mm; inside diameter (I.D.): 4 mm) packed with different catalysts with a particle size in the range of 250–425 μm, operated in a plug flow mode. The NTP was generated in a DBD reactor configuration via a tungsten wire placed in the centre of the quartz tube as the ground electrode, insulated within a sealed quartz capillary tube (O.D.: 1.8 mm) to prevent arcing, and the power electrode (aluminium foil) wrapped on the outer surface of the reactor. The length of the discharge was determined by the length of the foil and was kept constant for all the experiments at 2 cm. This ensured that the plasma region entirely covered the packed bed, irrespective of the materials used.

An alternating current power supply (PVM500 model) was used to ignite the plasma. The electrical parameters were monitored using an oscilloscope (Tektronix MDO3022) connected to the reactor using a high voltage probe (Tektronix P6015A) to measure the applied voltage and a probe to measure the plasma current using a 10 Ω resistor. An example of a voltage-current profile associated to the plasma is shown in Fig. 2. An electric air blower heater (LE Mini Sensor Kit) with controllable temperature and air pressure was used to supply the external heat to the DBD reactor when plasma reactions at elevated temperatures were required. The reactor temperature as a function of the heater temperature at a constant air pressure was calibrated by replacing the ground electrode with a K-type thermocouple inside the DBD reactor in the absence of plasma.

The reactor feed containing the desired gas mixtures of CH_4, O_2, CO, CO_2, NO, NH_3 and Ar/N_2 (all gas cylinders were supplied by BOC, 99.99% purity) was supplied using mass flow controllers (Bronkhorst El flow). The H_2O vapor was added to the feed gas stream by passing Ar/N_2 as a carrier gas through a custom-made saturator at specific

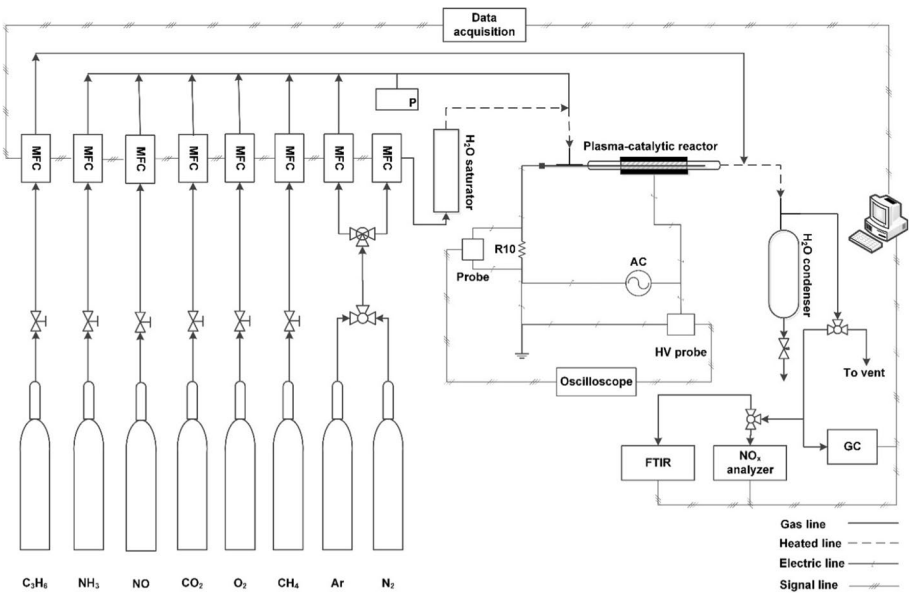

Fig. 1 Schematic of experimental setup

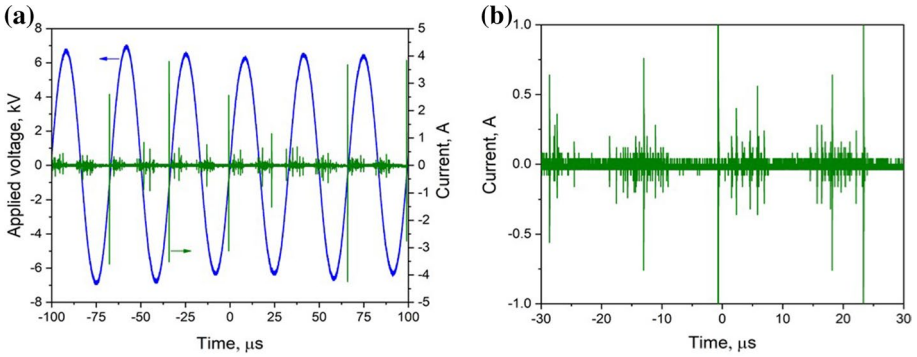

Fig. 2 **a** An example of voltage-current profile. **b** A zoomed-in plot of current in the range of − 30 μs–30 μs. Conditions: 7 kV, 30 kHz, 0.5 kPa CH_4, 10 kPa O_2 in N_2, gas hourly space velocity (GHSV) = 171,429 mL g^{-1} h^{-1}

temperature that was controlled using a Grant™ GD120 thermostatic bath. The produced water was removed from the gas stream after the reactor using a condenser, kept at 0 °C. All inlet and outlet gas lines were heat traced and maintained at 110 °C to prevent condensation. A gas chromatograph (GC; Agilent 7820A) was used to analyse the reactants and products and was equipped with a Porapak Q packed column and a flame ionization detector fitted with a methaniser to detect CO and CO_2. Propene, added post reactor and before the condenser to the effluent, was used as an internal standard. The concentration of NO_x was measured with a Signal 4000 VM series analyser equipped with a chemiluminescence detector. When NH_3 was added to the feed gas, a Bruker Vertex 70 FTIR spectrometer fitted with a gas cell with a volume of 190 cm^3 was used for the analysis of reactants and products. An additional catalyst bed for NH_3-SCR, consisting of Cu-CHA provided by Johnson Matthey Technology was used in these experiments.

Parameter Calculations

The average power consumed during the plasma process was calculated by Eq. (1). The instantaneous current was estimated by measuring the voltage across the resistor (V_r), placed on the ground region (see Fig. 1) and having the resistance (R), i.e. 10 Ω, according to Eq. (2).

$$P_{ave} = \frac{1}{T}\int_0^T V(t).I(t)\,dt \tag{1}$$

$$I(t) = \frac{V_r(t)}{R} \tag{2}$$

where I was the current, P_{ave} was the average power, t was time, T was a period, and V was the applied peak voltage. The specific input energy (SIE), representing the discharge energy density was calculated as the ratio of the average plasma power and the volumetric total gas flowrate at inlet.

$$\text{SIE} = \frac{\text{P}_{\text{ave}}}{\text{Volumetric total flowrate at inlet}} \quad (3)$$

In order to facilitate a comparison between plasma and thermal effects on the process an equivalent SIE for thermal systems was defined as the ratio of the thermal process heat duty (Q) in J s^{-1} and the volumetric total flowrate at inlet [20, 21].

$$\text{SIE} = \frac{Q}{\text{Volumetric total flowrate at inlet}} \quad (4)$$

The heat duty for the thermal systems was assumed to be the sensible heat needed to bring the temperature of the gaseous reactants to the final reaction temperature. This assumption was based on the fact that the discharge plasma power was measured according to the amount of energy injected to the plasma system without considering the energy of reactions [21]. The heat duty was calculated using the Eq. (5).

$$\text{Q} = \sum_{all\ reactants} \int_{T_r}^{T_f} C_P dT \quad (5)$$

where T_r was the room temperature (RT), T_f was the final reaction temperature and C_P was the heat capacity. The heat capacities for the gas components were calculated using equations from the literature (e.g. [34]) for an ideal gas state as a function of temperature.

The CH_4 conversion and product selectivity were calculated using Eqs. 6 and 7, respectively:

$$CH_4 \text{ conversion} = \frac{CH_4 \text{ molar flow rate at inlet - } CH_4 \text{ molar flow rate at outlet}}{CH_4 \text{ molar flow rate at inlet}} \quad (6)$$

$$\text{Product selectivity} = \frac{\text{Product molar flow rate at outlet}}{CH_4 \text{ molar flow rate at inlet - } CH_4 \text{ molar flow rate at outlet}} \quad (7)$$

Given the atmospheric conditions in this study, the reactant and product gases were assumed to follow ideal gas law. The carbon balance ($CH_4 + CO + CO_2$) was calculated and found to be close to 100% for all experiments. Only CO and CO_2 were observed as the carbon-based products for all the conditions investigated, therefore, the sum of CO and CO_2 selectivities were considered to be 100% to exclude small deviations. On the same basis, the CO_2 selectivity for experiments with CO_2 present in the feed was calculated using [CO_2 selectivity] = 100 − [CO selectivity].

The errors associated with CH_4 conversion, CO/CO_2 selectivity and NO_X formation in this study were ±5%, ±4% and ±91 ppmv, respectively. The thermodynamic calculations to assess the stable reaction products at various conditions were performed in Aspen Plus V9 using the built-in Gibbs reactor package.

Results and Discussion

Catalyst Screening

The CH_4 conversion, CO/CO_2 selectivity and SIE results for the different catalysts prepared are reported in Table 1. Note that, while the catalysts reported in Table 1 are screened

Table 1 The activity of various catalysts in NTP-assisted CH_4 oxidation at 7 kV and 30 kHz. Reaction conditions: 0.5 kPa CH_4, 10 kPa O_2 in N_2, GHSV = 85,714 mL g^{-1} h^{-1}

Catalyst	SIE, J mL^{-1}	CH_4 conversion, %	Selectivity, %	
			CO	CO_2
ZSM-5 (SiO_2/Al_2O_3 = 30)	5.4	48	60	40
ZSM-5 (SiO_2/Al_2O_3 = 80)	5.3	65	50	50
2 wt% Mo/ZSM-5 (SiO_2/Al_2O_3 = 30)	6.7	81	43	57
2 wt% Mo/ZSM-5 (SiO_2/Al_2O_3 = 80)	6.2	77	57	43
Al_2O_3	6.9	79	14	86
2 wt% Co/Al_2O_3	5.0	56	15	85
2 wt% Cu/Al_2O_3	4.9	48	8	92
2 wt% Fe/Al_2O_3	5.0	45	48	52
2 wt% Li/Al_2O_3	4.6	44	64	36
2 wt% Ni/Al_2O_3	4.7	45	41	59
2 wt% Pd/Al_2O_3	5.9	95	1	99
10 wt% Pd/Al_2O_3	5.1	99	1	99
2 wt% Pt/Al_2O_3	5.3	61	5	95
2 wt% Rh/Al_2O_3	5.4	46	8	92
2 wt% Ru/Al_2O_3	4.3	36	13	87

using one set of reaction conditions, the effect of varying the reaction conditions of the plasma-catalyst system is also further investigated for the best performing catalysts (see Sects. 3.2 and 3.3).

With zeolite-based materials, an increase in the molar SiO_2/Al_2O_3 ratio from 30 to 80 led to an increase in both CH_4 conversion and CO_2 selectivity from 48 to 65% and from 40 to 50%, respectively. The addition of Mo to both ZSM-5 (SiO_2/Al_2O_3 = 30 mol/mol) and ZSM-5 (SiO_2/Al_2O_3 = 80 mol/mol) enhanced the CH_4 conversion by 33% and 12% (up to 77% and 81%), respectively. The CO_2 selectivity stayed constant for the Mo/ZSM-5 (SiO_2/Al_2O_3 = 80 mol/mol) while for Mo/ZSM-5 (SiO_2/Al_2O_3 = 30 mol/mol), the CO_2 selectivity increased from 43 to 57%. The observed enhancement in conversion when Mo was added to the catalyst formulation could be related to the previously reported reactivity of molybdenum towards CH_4 activation [32, 35–40]. Mo/ZSM-5 has been applied to the methane aromatization reaction. This catalyst is bi-functional—methane is activated on the transition metal sites (Mo) to form intermediates which are further converted to aromatic compounds e.g. benzene on zeolite acidic sites [32]. As Mo is also active in partial oxidation reactions, e.g. oxidation of methanol to formaldehyde [36, 37], it is likely that in the presence of plasma, the methane could be partially oxidized and this could initiate a water gas shift-NTP reaction.

Over Al_2O_3, the NTP resulted in 79% CH_4 conversion and 86% CO_2 selectivity, a better performance when compared to the zeolite-based catalysts. Impregnating Pd on the Al_2O_3 support enhanced both the CH_4 conversion (up to 94–99%) and CO_2 selectivity (> 99%) with increasing precious metal loading (from 2 to 10 wt%). All other metals explored led to lower methane conversions than the pure alumina. The addition of Ru, Co, Cu, Rh and Pt led to a CO_2 selectivity similar or better than alumina; however, impregnation with Li, Fe or Ni resulted in significantly lower performance. It is likely that several reactions e.g. steam CH_4 reforming, partial oxidation, dry CH_4 reforming,

CO_2 methanation and H_2O-gas shift reaction occur simultaneously (with different rates) under the plasma-catalyst condition of this study, besides the CH_4 oxidation reaction (equations (S24) to (S35)). The active metals might promote side reactions resulting in an overall decrease in CO_2 selectivity and CH_4 conversion. For example, Gao et al. [41] have recently reported on the high-performance plasma enabled CO_2 methanation over bimetallic Ni–Fe catalysts using a nanosecond pulsed power supply. The low methane conversion and CO_2 selectivity observed with Fe, Li and Ni could indeed indicate that despite the known activity of these catalysts towards CO oxidation, in the presence of plasma, a number of side reactions take place.

As reported in Table 1, Pd/Al_2O_3 catalysts had the highest activity and selectivity in comparison to other catalysts tested. The Brunauer–Emmett–Teller (BET) surface area and X-ray diffraction (XRD) patterns for the Pd catalysts are reported in the ESI. It is noteworthy that Pd-based catalysts are known to have the best performance in thermal catalytic CH_4 oxidation [7, 42, 43]. Lee et al. [23] examined a 2 wt% Pd/Al_2O_3 powder catalyst in a fixed-bed reactor design during NTP-catalytic CH_4 oxidation at ambient temperature and obtained a significant increase in CH_4 conversion and CO_2 selectivity when adding the catalyst in the plasma zone, in line with the results of this study. Baylet et al. [22] compared the performance of post-plasma and in-plasma catalyst systems with plasma-only system for CH_4 combustion over a Pd/Al_2O_3/cordierite catalyst and reported that while CH_4 conversion remained the same for post-plasma catalyst and plasma-only systems, there was a significant decrease in CH_4 conversion for in-plasma catalyst system, attributed mainly to the lower residence time of the gas components when the catalyst was loaded in the discharge area. De Rosa et al. [21] reported a plasma-only, NTP-catalytic and thermal catalytic methane oxidation over a 2 wt% Pd/Al_2O_3 in 0.5 kPa CH_4, 10 kPa O_2, 5.5 kPa CO_2, 7 kPa H_2O in N_2 using a different reactor configuration, i.e. an alumina tube reactor with a stainless steel wire as the internal electrode, in comparison to the reactor configuration of this study. No synergistic effect on CH_4 conversion was observed when combining plasma and catalyst with an AC power supply although there was a synergistic effect on CH_4 conversion using a nanopulse power supply [21] and similar findings were reported by Nozaki et al. [26].

In-situ DRIFTS-MS studies revealed that the formation of surface species, e.g. carbonate and formate, was significantly affected by the plasma in the methane oxidation over a Pd catalyst in comparison to the thermal catalytic reactions [25]. In addition, temperature increases in the NTP-catalyst system have been observed and it was suggested that this process was not isothermal especially at high plasma SIEs [21, 24, 44]. De Rosa et al. [21] reported a linear relationship between the reactor temperature (up to 300 °C) and the SIE in the plasma-only and plasma catalyst systems. Molteni et al. [44] reported that the temperature rise induced by the plasma was significant during CH_4 oxidation reaction and this might lead to increased methane conversion. However, Gibson et al. [24] reported that the temperature rise in the bed was insufficient to lead to the thermal catalytic CH_4 conversion. Using an IR camera and EXAFS, it was found that during the CH_4 oxidation over a Pd/Al_2O_3 catalyst packed in the NTP zone, the temperature of the Pd nanoparticles was around 162 °C, i.e. below the temperature required for the activation of CH_4 (> 200 °C) [24]. The heat generated during plasma-induced CH_4 oxidation reaction, on the other hand, might promote the further oxidation of CO to form CO_2 over the catalyst, because temperatures below 200 °C are sufficient for CO oxidation over Pd/Al_2O_3 catalysts [45, 46].

The calculated SIE results, shown in Table 1, varied in the range of 4.3–6.9 J mL^{-1} for different catalyst system even though the experiments in Table 1 were conducted under apparently identical reaction conditions (e.g. constant applied voltage and frequency). The

metals impregnated on the catalyst surface might be the source of variations in SIEs by changing the dielectric constant in the discharge zone [47].

Effect of Gas Components and GHSV

The effect of the reactant feed gas composition and GHSVs on the CH_4 conversion and CO/CO_2 selectivity over Al_2O_3 and 10 wt% Pd/Al_2O_3 catalyst is reported in Fig. 3. To further differentiate the effect of Pd metal on Al_2O_3 support, a catalyst with a higher loading of Pd (10 wt% Pd/Al_2O_3) was selected for the rest of study. The gas compositions consisted of:

- Condition (a): 0.5 kPa CH_4, 10 kPa O_2 in Ar;
- Condition (b): 0.5 kPa CH_4, 10 kPa O_2 in N_2;
- Condition (c): 0.5 kPa CH_4, 10 kPa O_2, 7 kPa H_2O, 5.5 kPa CO_2 and 0.1 kPa NO, in N_2.

With Ar as the balance gas, the conversion of CH_4 over the 10 wt% Pd/Al_2O_3 is high, e.g. 98% at GHSV = 171,429 mL g^{-1} h^{-1}, and significantly higher than over Al_2O_3 at the same GHSV, e.g. 59% at GHSV = 171,429 mL g^{-1} h^{-1}. An increase in the GHSV in the plasma-catalyst system reduced the overall residence time of the gas components, and the energy density, resulting in, as expected, lower conversions. As observed in Fig. 3, doubling the GHSV from 171,429 to 342,858 mL g^{-1} h^{-1} decreased the CH_4 conversion slightly for the 10 wt% Pd/Al_2O_3 from 98 to 96% and, significantly for Al_2O_3 from 59 to 43%. The CO_2 selectivity remained around 100% over the 10 wt% Pd/Al_2O_3 and decreased from 89 to 78% for Al_2O_3. It is believed that besides the electron-impact dissociation of CH_4 and O_2 in the plasma, the excited Ar species can dissociate CH_4 and O_2 through a "Penning dissociation" phenomenon which correlates to an energy transfer from excited species to other molecules [15, 48, 49]. The relatively small decrease in

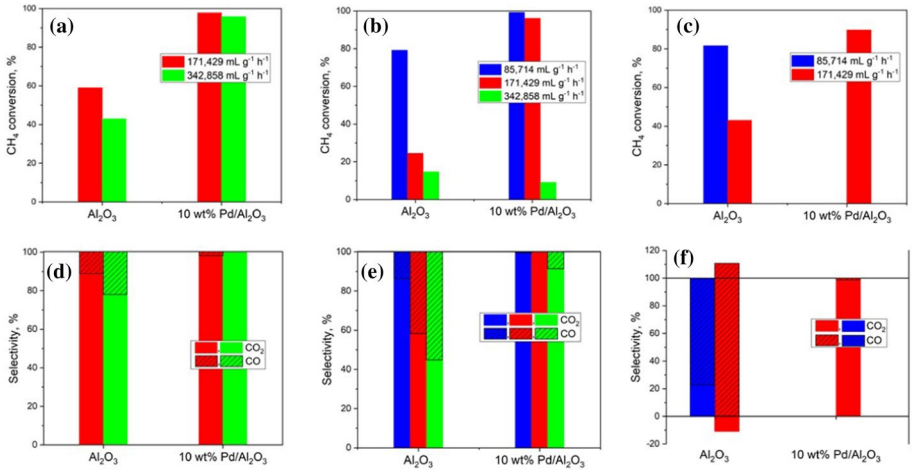

Fig. 3 Effect of feed gas composition and GHSV on NTP-catalytic CH_4 oxidation over 10 wt% Pd/Al_2O_3 at 7 kV, 30 kHz. (**a** and **d**) Condition (a): 0.5 kPa CH_4, 10 kPa O_2 in Ar; (**b** and **e**) Condition (b): 0.5 kPa CH_4, 10 kPa O_2 in N_2; (**c** and **f**) Condition (c): 0.5 kPa CH_4, 10 kPa O_2, 7 kPa H_2O, 5.5 kPa CO_2 and 0.1 kPa NO in N_2

conversion of methane when increasing the GHSV could be attributed to the kinetically enhanced collisions between the excited noble gas atoms and methane molecules. As shown in Fig. 3b, if the GHSV is further increased, the positive effect of the gas phase chemistry is superseded by the reaction kinetics over the catalyst, represented by a ~ ten-fold reduction in CH_4 conversion at the highest space velocity.

The impact of using N_2 as the balance gas on the CH_4 conversion was assessed with condition (b). At a similar GHSV, there was a decrease in the CH_4 conversion for both 10 wt% Pd/Al_2O_3 and Al_2O_3 catalysts when using N_2 instead of Ar as balance. The effect of N_2 was more pronounced at high GHSVs, e.g. at 342,858 mL g^{-1} h^{-1}, the CH_4 conversion decreased from 96% for condition (a) to almost 10% for condition (b) over the 10 wt% Pd/Al_2O_3 catalyst. As discussed above, the Penning effect can account, to a certain extent, for the higher CH_4 conversion in Ar. While CO_2 selectivity remained above 90% over the 10 wt% Pd/Al_2O_3 for both conditions (a) and (b), it decreased significantly over the Al_2O_3 catalyst when replacing Ar with N_2 at a constant GHSV. For example, the CO_2 selectivity reduced from 89% at condition (a) to 58% at condition (b) when GHSV was 171,429 mL g^{-1} h^{-1} and Al_2O_3 was used as the catalyst.

Modeling studies for a mixture of $CO_2/CH_4/N_2$ (1:1:8) have shown that the dissociation of CH_4 and CO_2 splitting to CO and O are promoted by the metastable singlet and triplet states generated by electron impact excitation of N_2, which enhances CH_4 and CO_2 conversions [50] (equations listed in ESI, Section S2). This effect is not observed for CH_4 conversion in this study but the decrease in CO_2 selectivity over Al_2O_3 by switching to N_2 balance could be attributed to the collision of some of the generated CO_2 molecules with metastable N_2.

When a complex gas mixture containing CH_4, O_2, CO_2, H_2O, NO and N_2 balance [condition (c)] was tested over the 10 wt% Pd/Al_2O_3 catalyst, the methane conversion remained high, with less than 10% decrease compared to the simpler gas mixtures used in conditions (a) and (b). For example, at a GHSV of 171,429 mL g^{-1} h^{-1} when changing the feed composition from condition (a) to (b) and (c), the methane conversion was 97.7, 96.1 and 89.7%, respectively, while the CO_2 selectivity remained very high (above 98%) in all cases. In contrast, when using Al_2O_3, the CH_4 conversion increased in condition (c) compared with condition (b), from 25 to 43% at GHSV of 171,429 mL g^{-1} h^{-1}. In line with the Al_2O_3 results, an improvement in CH_4 conversion using condition (c) gas was also observed in comparison to condition (b). However, the CO_2 selectivity reduced significantly when switching to condition (c) over Al_2O_3 compared with condition (b), from 58% to − 11% at GHSV of 171,429 mL g^{-1} h^{-1}. Note that the negative CO_2 selectivity indicates that some of the inlet CO_2 was converted during the plasma reaction, for example through methane reforming, as discussed in [22]. This would be consistent with the observed increase in CO selectivity.

Under thermal conditions, it is known that the Pd catalyst activity is inhibited by the presence of combustion products e.g. H_2O or CO_2 [6, 42] which may also be the reason for the small decrease in conversion under NTP conditions observed with the 10 wt% Pd/Al_2O_3 catalyst. Similarly, the addition of H_2O to the plasma-assisted catalytic toluene oxidation was shown to have a negative effect on catalyst activity, and was attributed to the competitive adsorption of water and also to a change in the plasma discharge behavior through quenching energetic electrons and reactive species [51, 52]. However, a previous study observed a promotional effect of H_2O addition to the plasma-assisted catalytic CO oxidation through facilitating the decomposition of carbonate species on the Cu/Ce catalyst and enhancing catalyst stability [53].

When considering different feed compositions and reaction conditions, it can be concluded that, for the current study, a promotional effect of the addition of Pd compared to the support alone was also observed, both in terms of CH_4 conversion and CO_2 selectivity.

Effect of External Heat Supply and Plasma Energy

To evaluate the effect of combining an external heat source with the NTP to activate the catalyst for the CH_4 oxidation reaction, a heat blower was used to control the reactor temperature up to 300 °C. The performance of the NTP-catalytic CH_4 oxidation over the 10 wt% Pd/Al_2O_3 with a feed composition of 0.5 kPa CH_4, 10 kPa O_2, 7 kPa H_2O, 5.5 kPa CO_2 and 0.1 kPa NO in N_2 as a function of reactor temperature and plasma SIE is reported in Fig. 4. The variation in plasma SIE from 1.1 to around 4.9 J mL^{-1} is the result of a change in the applied peak voltage from 5 to 7 kV at a constant frequency of 30 kHz. The plasma SIE followed a linear relationship with the applied voltage as shown in Fig. S2. As the applied voltage increased there was also an increase in the reactor temperature which contributed to a small increase in the plasma SIE, presented in Fig. S3. For example, at 7 kV and 30 kHz, the plasma SIE increased from around 3.7 to 4.7 J mL^{-1} when the temperature increased from RT to 300 °C.

Because CH_4 is a more stable molecule compared to other hydrocarbons, due to the strength of the C–H bonds, it requires high temperatures or energies to be activated. Typically, the thermal catalytic CH_4 oxidation over supported Pd catalysts is initiated at temperatures above 200 °C and often only reaches 100% CH_4 conversion at 400 °C or above [24, 42]. Examining CH_4 oxidation reaction over the 10 w% Pd/Al_2O_3 at the operating conditions shown in Fig. 4, in the thermal mode (no plasma), no CH_4 conversion from RT to 250 °C took place and only 4% CH_4 conversion was observed at 300 °C. The limited CH_4 conversion at 300 °C in this study may be attributed to the presence of H_2O and CO_2 in the gas feed which act as poisons [6, 42]. From Fig. 4a it is observed that an increase in plasma SIE and temperature led to an enhancement of the CH_4 conversion. For example, at a constant plasma SIE of 1.5 J mL^{-1}, an increase in temperature from RT to 300 °C increased the CH_4 conversion from 0 to 98%. Similarly, without external heat supply (at RT in Fig. 4a), increasing the plasma SIE from 1.2 to 3.7 J mL^{-1} improved the CH_4

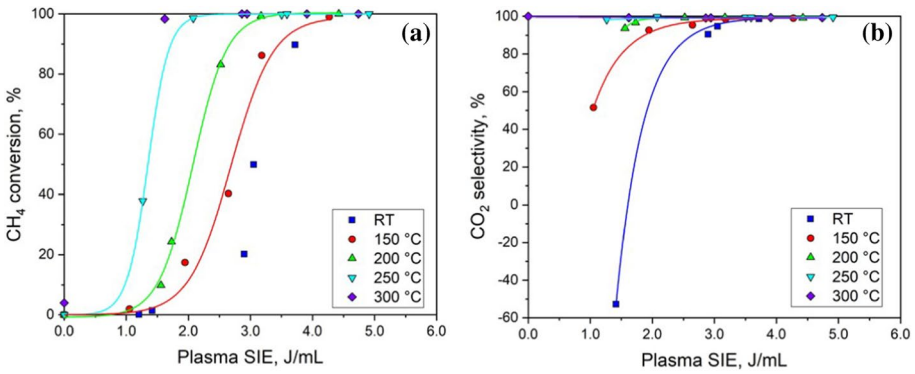

Fig. 4 CH_4 conversion (**a**) and CO_2 selectivity (**b**) as a function of temperature and plasma SIE in NTP-catalytic CH_4 oxidation (the lines are only to guide the eye). Reaction conditions: 10 wt% Pd/Al_2O_3, 0.5 kPa CH_4, 10 kPa O_2, 7 kPa H_2O, 5.5 kPa CO_2 and 0.1 kPa NO in N_2, 171,429 mL g^{-1} h^{-1} GHSV

conversion from almost 0 to 90%. The plasma-assisted catalytic process without external heat contribution can activate CH_4 at RT and very high conversion of CH_4 to products can be achieved with an increase in plasma SIE. Similar effect of the plasma SIE on CH_4 conversion during plasma-only CH_4 oxidation was reported [23].

Increasing the plasma SIE and temperature also enhanced the CO_2 selectivity over the 10 wt% Pd/Al_2O_3 catalyst as shown in Fig. 4b. The CO_2 selectivity was above 90% once the CH_4 conversion was greater than 10%. Once the Pd catalyst became activated in the reaction, through heat supply or plasma, the CO_2 selectivity reached around 100%. Conversely, at low temperatures (< 150 °C) and plasma SIEs (e.g. 1.1 J mL^{-1}) where the CH_4 conversion is below 10%, other reactions such as steam reforming of methane or dry reforming of methane govern the conversion, as also discussed in Sect. 3.2, and resulted in negative or low CO_2 selectivities. In agreement with these results, Pham Huu et al. [28] reported a shift in CH_4 conversion towards lower light-off temperatures when using plasma-assisted catalytic CH_4 oxidation with in-plasma and post-plasma configurations in comparison to thermal catalytic reaction and plasma alone.

To achieve the same level of CH_4 conversion in a plasma-catalyst system, the applied peak voltage and reactor temperature can be tuned, as shown in Table 2. From an energy perspective, increasing the external heat supply significantly reduced the plasma energy and total energy required to obtain the same CH_4 conversion. For example, the plasma SIE required to obtain 50% CH_4 conversion, reduced from 3.1 to 1.3 J mL^{-1} resulting in the total SIE reducing from 3.1 to 1.6 J mL^{-1} when the temperature increased from RT to 260 °C, respectively. Similarly, a decrease in plasma SIE from 3.7 to 1.6 J mL^{-1} required an increase in the temperature from RT to 293 °C to obtain 90% CH_4 conversion at the reactor outlet, leading to a decrease in total SIE from 3.7 to 1.9 J mL^{-1}. In summary, a combination of plasma and external heat supply in a plasma-catalyst gives access to high CH_4 conversion with lower energy consumption.

The results in Table 2 also indicate that the external heat is more efficient than the plasma at initiating the methane oxidation reaction, in line with the results reported by [21]. However, it is worth noting that, in a practical application, the heat is dependent on the exhaust gas temperature, which leads to inefficient cold start emission control using traditional approaches. Under such conditions, where the heat supply is low, plasma could be used as it is almost instantaneous in its onset. As shown in Fig. S4, a process control with time dependent regulation (decrease) of the plasma SIE could guarantee methane emission abatement while minimizing the energy penalty by tuning the SIE from the NTP.

Table 2 Obtaining the same level CH_4 conversion as a function of temperature and applied voltage. Data were extracted from Fig. 4

50% CH_4 conversion					90% CH_4 conversion				
Applied voltage, kV	Temperature, °C	SIE, J mL^{-1}			Applied voltage, kV	Temperature, °C	SIE, J mL^{-1}		
		Thermal	Plasma	Total			Thermal	Plasma	Total
6.5	RT	0	3.1	3.1	7.0	RT	0	3.7	3.7
6.0	161	0.17	2.6	2.8	6.5	164	0.17	3.2	3.4
5.5	217	0.24	1.8	2.0	6.0	221	0.24	2.9	3.1
5.0	260	0.29	1.3	1.6	5.5	244	0.27	2.0	2.3
–	–	–	–	–	5.0	293	0.33	1.6	1.9

Table 3 CH_4 conversion and NO_X formation in plasma discharge; 7 kV, 30 kHz, 0.5 kPa CH_4, 10 kPa O_2 in N_2, GHSV = 171,429 mL g^{-1} h^{-1}

Catalyst	CH_4 conversion %	NO ppmv	NO_2 ppmv	NO_X ppmv	NO/NO_2
Al_2O_3	25	388	257	644	1.51
10% Pd/Al_2O_3	96	524	311	836	1.68

Table 4 CH_4 conversion and NO_X formation in plasma discharge as function of reaction conditions over 10 wt% Pd/Al_2O_3 at 7 kV, 30 kHz. All conditions were tested at GHSV of 171,429 mL g^{-1} h^{-1}

Condition	Temperature, °C	Feed gas composition	CH_4 conversion, %	Outlet NO_X concentration, ppmv
b	RT	0.5 kPa CH_4 and 10 kPa O_2 in N_2	96	836
c	RT	0.5 kPa CH_4, 10 kPa O_2, 5.5 kPa CO_2, 7 kPa H_2O and 0.1 kPa NO in N_2	90	1224
d	300	0.5 kPa CH_4, 10 kPa O_2, 5.5 kPa CO_2, 7 kPa H_2O and 0.1 kPa NO in N_2	100	1714

NOX Production and Mitigation Strategies

Together with the CH_4 conversion and CO_2 selectivity, the effect of plasma on NO_X formation/conversion needs to be considered in after-treatment applications. The presence of N_2 as the balance gas resulted in the production of a combination of NO and NO_2 in the plasma discharge zone (Table 3). The amount of NO_X produced was 836 ppmv in the presence of the Pd/Al_2O_3 catalyst while the use of Al_2O_3 support in the plasma zone resulted in a decrease in NO_X formation to 644 ppmv. These changes also reflected changes in the CH_4 conversion with high NOx formation occurring at high CH_4 conversions, as a result of the increase in electric field intensity. This consequently lead to an increase in the rate of formation of active species (such as N, O, CH_3) through electron impact reactions, and the effective collisions between them (equations listed in ESI, section S2). Moreover, the NO/NO_2 ratio also varied and increased in the following order: $Al_2O_3 < Pd/Al_2O_3$. Under the conditions of this study, thermodynamic calculations suggest that only NO is a stable product of N_2 and O_2 reaction, especially at high SIEs. This indicates that the plasma provides non-equilibrium conditions with generation of a mixture of NO and NO_2.

The effect of the reaction conditions on the CH_4 conversion and NO_X formation over the 10 wt% Pd/Al_2O_3 is reported in Table 4. Under condition (c), the feed gas contained 1000 ppmv NO_X (corresponding to 0.1 kPa NO) and the effluent data indicated the formation of an additional 224 ppmv NO_X during the plasma-catalytic reaction. This reflected a decrease in the amount of NO_X formed in the plasma in comparison to condition (b) due to the addition of NO in the feed gas. These preliminary results seemed to indicate that the presence of NO in the feed gas led to reduced formation of NO_X. However, when the reactor temperature was increased to 300 °C (condition (d)), the formation of NO_X in the DBD increased to 714 ppmv, to a total of 1714 ppmv outlet concentration. This is consistent with the reported formation of NO_X (mainly from plasma gas phase reactions via Eqs. (8, 9, 10, 11, 12, and 13))

being enhanced even if NO is already present in the feed. These results are in good agreement with those reported in [54], which attributed this behaviour to the fact that a 10% oxygen concentration in the feed is above the critical oxygen concentration range, leading to an increase in the NO_X concentration with the energy density. The present results also indicate that the energy density dependence is driven by both the plasma and heat. The general trend reported in Fig. 5 appears to indicate a good correlation between the CH_4 conversion and the effluent NO_X concentration, for all the catalysts tested in this study, irrespective of reaction conditions. The results, herein, also indicate that the simultaneous NO_X reduction and methane oxidation is not possible within the conditions investigated due to the electron impact dissociation of N_2 and O_2 (Eqs. (8, 9, and 10)) and the subsequent reactions that occur between the active species, some of which are listed in ESI Section S2 [22, 50–56].

$$e^- + N_2 \rightarrow e^- + N + N \tag{8}$$

$$e^- + O_2 \rightarrow e^- + O + O \tag{9}$$

$$e^- + NO \rightarrow e^- + O + N \tag{10}$$

$$O + O_2 \rightarrow O_3 \tag{11}$$

$$N + O_2 \rightarrow NO + O \tag{12}$$

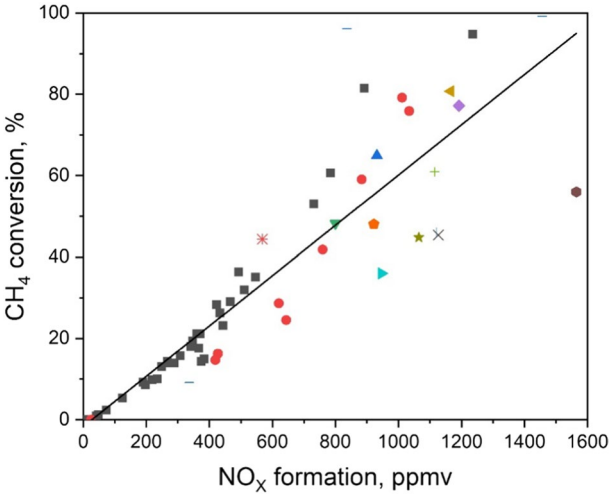

Fig. 5 CH_4 conversion as a function of NO_X formation over all catalysts tested in this study at different reaction conditions. Note NO is not added to the gas feed in any of the tests in this figure. (Green Inverted triangle) ZSM-5 ($SiO_2/Al_2O_3 = 30$); (Blue triangle) ZSM-5 ($SiO_2/Al_2O_3 = 80$); (Golden brown Left pointer triangle) 2 wt% Mo/ZSM-5 ($SiO_2/Al_2O_3 = 30$); (Diamond) 2 wt% Mo/ZSM-5 ($SiO_2/Al_2O_3 = 80$); (Red circle) Al_2O_3; (Brown Hexagon) 2 wt% Co/Al_2O_3; (Orange pentagon) 2 wt% Cu/Al_2O_3; (Star) 2 wt% Fe/Al_2O_3; (Orange asterisk) 2 wt% Li/Al_2O_3; (Multiplication symbol) 2 wt% Ni/Al_2O_3; (Black square box) 2 wt% Pd/Al_2O_3; (Minus symbol) 10 wt% Pd/Al_2O_3; (Plus symbol) 2 wt% Pt/Al_2O_3; (Vertical blue line) 2 wt% Rh/Al_2O_3; (Cyan right pointer triangle) 2 wt% Ru/Al_2O_3 (Color figure online)

$$O + N \rightarrow NO \tag{13}$$

To address this challenge and to mitigate for the NO_X formation, a different approach was explored, whereby the addition of ammonia and a suitable SCR catalyst was considered. While NH_3-SCR (Eqs. (14, 15, and 16)) is a mature technology, it is not suitable for simultaneous conversion of methane and NO_X under realistic conditions during cold start [57].

$$4NH_3 + 6NO \rightarrow 5N_2 + 6H_2O \text{ slow SCR} \tag{14}$$

$$4NH_3 + 2NO + 2NO_2 \rightarrow 4N_2 + 6H_2O \text{ fast SCR} \tag{15}$$

$$4NH_3 + 4NO + O_2 \rightarrow 4N_2 + 6H_2O \text{ standard SCR} \tag{16}$$

The catalyst of choice for the SCR process is a commercially available system, Cu-CHA from Johnson Matthey Technology. A typical thermal activation light-off experiment is reported in Fig. 6. As expected and reported in the literature [58], the activity of the Cu-CHA catalyst for NO_X reduction was found to be high, with 100% conversion achieved at 190 °C under standard thermal activation. As noted earlier, the conversion of methane under these conditions is negligible below 400 °C, as illustrated in Fig. 6. Thus, an assessment of the effect of plasma on the simultaneous reduction of NO_X and CH_4 oxidation during cold start using NH_3 as a reducing agent was examined.

For a better understanding of the formation and evolution of the reaction products/intermediates during the plasma exposure, without the interference from high concentrations of H_2O and CO_2, the inlet feed was simplified (CH_4, O_2, NO and NH_3 with N_2 balance) and the outlet line of the reactor was connected directly to an FTIR. The following vibrational bands were used as diagnostics for the presence of different species: CH_4 at 3016 and 1304 cm^{-1}, CO_2 at 2360 cm^{-1}, CO at 2143 cm^{-1}, NO at 1883 cm^{-1}, NO_2 at 1614 cm^{-1}, N_2O at 2223 cm^{-1}, HNO_3 at 1325 and 1718 cm^{-1} [56].

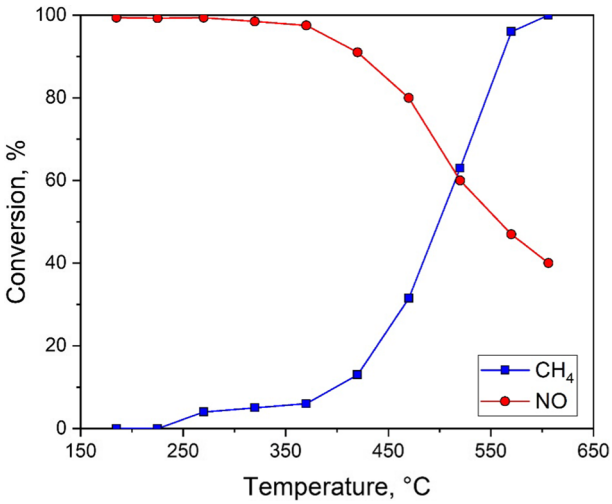

Fig. 6 NO (red) and CH_4 conversions (blue) as function of reactor temperature using a commercial Cu-CHA catalyst. Reaction conditions: 0.5 kPa CH_4, 10 kPa O_2, 0.1 kPa NO, and 0.1 kPa NH_3 in Ar, GHSV = 85,714 mL g^{-1} h^{-1} (Color figure online)

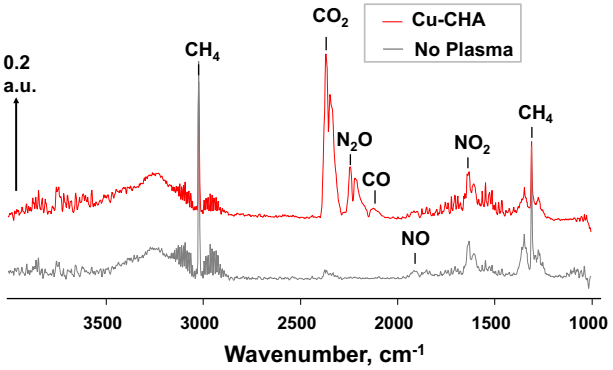

Fig. 7 FTIR spectra for inlet feed and final reactor products with Cu-CHA catalyst in the DBD. Reaction conditions: 0.5 kPa CH_4/10 O_2/0.1 NO/0.1 NH_3 in N_2

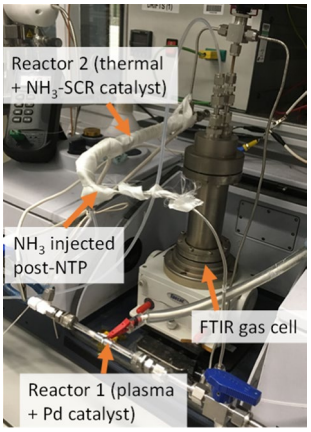

Fig. 8 Experimental setup for CH_4 oxidation using plasma-catalyst and thermal NH_3-SCR post-plasma treatment

Figure 7 reports the FTIR spectra of the reactants and products from the DBD reactor with the addition of Cu-CHA to the discharge, at 2.1–2.3 J mL^{-1}. When the plasma is ignited, a 40% reduction in the methane concentration was observed and a decrease in the intensity of NO band. However, since the NO_2 concentration simultaneously increased, very little change was observed in the overall NO_X conversion indicating that the NO was oxidised to NO_2. This is in good agreement with [54]. Nitrous oxide was also formed in the plasma discharge (equations (S6) to (S9)), with concentration of approximately 430 ppmv N_2O. Wang and Tokunaga [54, 59] reported that in the presence of a high concentration of O radicals and O_2, both NO_X and N_2O are formed in plasma (equations (S1) to (S25)). It should, however, be noted that the increase of the peaks at 2210–2250 cm^{-1} might not be entirely due to N_2O formation, but also to other -NCO species.

To prevent the NH_3 from being oxidised in the plasma instead of being utilised as a reducing agent, a hybrid solution was further explored. It made use of a hybrid dual-stage reactor where the oxidation reactions took place upstream in the plasma discharge (in-plasma catalysis (IPC)) and the SCR catalyst and NH_3 injection were located downstream, i.e. in a post-plasma catalysis (PPC) configuration, as shown in Fig. 8 (with further details in Fig. S5). This configuration benefited from the supply of a small amount of heat from the methane oxidation zone to the SCR region.

The dual stage configuration resulted in a full methane conversion with > 99% CO_2 selectivity, as evidenced in Fig. 9 from the disappearance of the bands at 3016 and 1304 cm^{-1}, and the increase of the CO_2 feature at 2360 cm^{-1}, respectively. Once NH_3 was injected downstream of the plasma reactor, the NO_X were fully converted, as shown by the disappearance of the NO and NO_2 bands. No significant change was observed in the intensity of the band at 2223 cm^{-1} when compared to the one in Fig. 7 (417 ppmv N_2O), which indicated that this species is produced in the plasma discharge and the catalysts used herein did not promote the formation nor the removal of this product. Zhao et al. [60] have shown a strong correlation between the SIE and N_2O formation when a V_2O_5-WO_3/TiO_2 catalyst was used. In our previous study on HC-SCR [19] we have shown that the N_2O selectivity is dependent on the applied frequency, temperature and NOx conversion and we have proposed that the duration of the pulse can be of high importance, as also discussed by de Rosa et al. [21] While N_2O slip is highly undesirable, the current study was not intended for exhaustive mitigation strategies but rather to put forward a possible solution for cold-start CH_4 and NO_X emission control for diesel engines.

As demonstrated in the present study, the main disadvantage of using an in-plasma catalyst discharge to reach complete oxidation of the methane under realistic exhaust conditions was the formation or low conversion of NO_X (Eqs. (8, 9, 10, 11, 12, and 13) and (S1) to (S25)).

It was found that the concentration of oxygen in the feed had a critical role on the NTP denitration performance [54] and, while high conversions of NO_X can be achieved with O_2 concentration lower than 1%, this is not realistic for automotive exhaust conditions. It is important to note that the addition of water and ammonia is beneficial towards the NO_X removal efficiency even with O_2 concentrations > 10% as long as the SIE is kept below 2 J mL^{-1}, as shown by Wang et al. It is suggested that, as soon as the SIE increases, allowing for more reactive oxygen species (ROS) to be formed, the removal efficiency becomes negative, with reactions (Eqs. (12), (13)) more prone to take place. Furthermore, the interaction between the excited NO* and other N-containing species formed in the plasma and on the oxide ions at the catalyst surface, gives rise to $–NO_X$ and $–NO_2$ species, which could lead to an increase in the overall NO_X concentration, resulting therefore in a negative NO_X removal efficiency [54, 61]. The ease of –N radicals formation is of paramount importance in terms of NO_X concentration and it might be that a different way of generating plasma

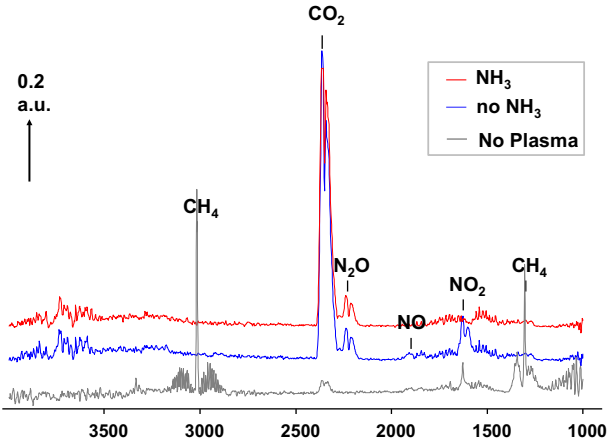

Fig. 9 FTIR spectra for final reaction products of the dual stage reactor. 0.5% CH_4/10% O_2/0.1% NO/0 (blue)–0.1% (red) NH_3/N_2; GHSV = 85,714 mL g^{-1} h^{-1}; 70 mg 10% Pd/Al_2O_3; 70 mg Cu-CHA catalyst downstream plasma discharge, 190 °C reaction temperature (Color figure online)

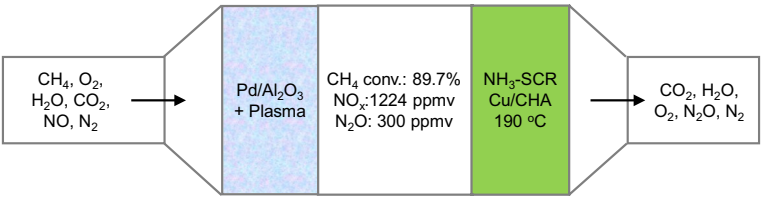

Fig. 10 Proposed solution for simultaneous CH_4 and NO_X conversion for Diesel cold start

instead of the DBD method could indeed lead to significant differences in NO_X concentration, as seen in [54].

The properties observed for the combined hybrid system indicate that the use of the NTP + catalyst closely followed by an ammonia-SCR system may hold the solution to diesel cold start emission control, as proposed in Fig. 10.

Conclusions

This paper reports on the NTP-catalytic methane oxidation as an aftertreatment technology to remove methane emissions in the exhaust of methane-powered vehicles. High CH_4 conversion and CO_2 selectivities can be achieved with the presence of a catalyst in a DBD reactor. The CO_2 selectivity during NTP-catalytic CH_4 oxidation is related to the CH_4 conversion and increases linearly with the CH_4 conversion. In agreement with thermal catalysis, Pd/Al_2O_3 catalysts are shown to have the best performance for the NTP-catalytic methane oxidation in terms of CH_4 conversion and CO_2 selectivity among all catalysts tested. The performance of the plasma-catalyst system is found to depend on feed gas components and GHSVs. Complex gas mixtures that simulate real exhaust conditions can reduce methane conversion when using Pd/Al_2O_3 catalysts. A combination of plasma and external heat supply in a plasma-catalyst system can achieve high CH_4 conversion and CO_2 selectivity with lower energy consumption. This is an approach that appears particularly suitable to cold-start conditions using biogas as a fuel. The presence of N_2 and O_2 in the plasma system can lead to unfavorable NO_X formation, which is not preventable as long as the plasma exists due to electron-impact dissociation reaction of these molecules. The NO_X formation has a linear dependence with CH_4 conversion during NTP-catalytic CH_4 oxidation. The addition of a second catalyst bed, post-plasma, where NH_3 can be injected for selectively reduce the nitrogen oxides at temperatures below 200 °C was shown to be an efficient solution in this case.

It is concluded that the most suitable aftertreatment option involves the combination of an oxidation catalyst with plasma to target the hydrocarbon and CH_4 oxidation, followed by the NH_3-SCR system to convert the NO_X.

Supplementary Information The online version contains supplementary material available at https://doi.org/10.1007/s11090-022-10253-3.

Acknowledgements The authors acknowledge funding from Innovate UK under grant ref: 102661. Open access data can be found via the University of Manchester research portal.

Author Contributions RG: Investigation, Writing-Original draft preparation, Writing-Reviewing and editing; CS: Investigation, Methodology, Writing-Reviewing and editing; SC: Validation, Writing-Reviewing

and editing; AS: Investigation, Validation; AG: Conceptualization, Funding acquisition, Writing-Reviewing and editing; PH: Supervision, Funding acquisition; PM: Funding acquisition, Project administration; CH: Conceptualization, Funding acquisition, Project administration, Supervision, Validation, Writing-Reviewing and editing.

Declarations

Conflict of interest The authors report no declaration of interest.

References

1. Curran SJ, Wagner RM, Graves RL et al (2014) Well-to-wheel analysis of direct and indirect use of natural gas in passenger vehicles. Energy 75:194–203. https://doi.org/10.1016/j.energy.2014.07.035
2. Torchio MF, Santarelli MG (2010) Energy, environmental and economic comparison of different powertrain/fuel options using well-to-wheels assessment, energy and external costs–European market analysis. Energy 35:4156–4171. https://doi.org/10.1016/j.energy.2010.06.037
3. U.S. Department of Energy (2021) Alternative fuels data center: natural gas vehicles. https://afdc.energy.gov/vehicles/natural_gas.html
4. U.K. Department of Transport (2015) RICARDO-AEA provision of HGV emissions testing, RM4470-SB2925. https://assets.publishing.service.gov.uk/government/uploads/system/uploads/attachment_data/file/468172/hgv-emissions-testing.pdf
5. Gélin P, Urfels L, Primet M, Tena E (2003) Complete oxidation of methane at low temperature over Pt and Pd catalysts for the abatement of lean-burn natural gas fuelled vehicles emissions: influence of water and sulphur containing compounds. Catal Today 83:45–57. https://doi.org/10.1016/S0920-5861(03)00215-3
6. Gholami R, Alyani M, Smith K (2015) Deactivation of Pd catalysts by water during low temperature methane oxidation relevant to natural gas vehicle converters. Catalysts 5:561–594. https://doi.org/10.3390/catal5020561
7. Cargnello M, Jaén JJD, Garrido JCH et al (2012) Exceptional activity for methane combustion over modular Pd@CeO_2 subunits on functionalized Al_2O_3. Science 337:713–717. https://doi.org/10.1126/science.1222887
8. Coney C, Stere C, Millington P et al (2020) Spatially-resolved investigation of the water inhibition of methane oxidation over palladium. Catal Sci Technol 10:1858–1874. https://doi.org/10.1039/D0CY00154F
9. Neyts EC, Ostrikov K, SunkaraBogaerts MKA (2015) Plasma catalysis: synergistic effects at the nanoscale. Chem Rev 115:13408–13446. https://doi.org/10.1021/acs.chemrev.5b00362
10. Azzolina-Jury F, Bento D, Henriques C, Thibault-Starzyk F (2017) Chemical engineering aspects of plasma-assisted CO_2 hydrogenation over nickel zeolites under partial vacuum. J CO2 Util 22:97–109. https://doi.org/10.1016/j.jcou.2017.09.017
11 Patil BS, Cherkasov N, Lang J et al (2016) Low temperature plasma-catalytic NO_X synthesis in a packed DBD reactor: effect of support materials and supported active metal oxides. Appl Catal B Environ 194:123–133. https://doi.org/10.1016/j.apcatb.2016.04.055
12. Uytdenhouwen Y, Bal KM, Neyts EC et al (2021) On the kinetics and equilibria of plasma-based dry reforming of methane. Chem Eng J 405:126630. https://doi.org/10.1016/j.cej.2020.126630
13 Khoja AH, Tahir M, Amin NAS (2019) Recent developments in non-thermal catalytic DBD plasma reactor for dry reforming of methane. Energy Convers Manag 183:529–560. https://doi.org/10.1016/j.enconman.2018.12.112

14. Ahmad F, Lovell EC, Masood H et al (2020) Low-temperature CO_2 methanation: synergistic effects in plasma-Ni hybrid catalytic system. ACS Sustain Chem Eng 8:1888–1898. https://doi.org/10.1021/acssuschemeng.9b06180
15. Vakili R, Gholami R, Stere CE et al (2020) Plasma-assisted catalytic dry reforming of methane (DRM) over metal-organic frameworks (MOFs)-based catalysts. Appl Catal B Environ 260:118195. https://doi.org/10.1016/j.apcatb.2019.118195
16. Wang H, Zhao B, Qin L et al (2020) Non-thermal plasma-enhanced dry reforming of methane and CO_2 over Ce-promoted Ni/C catalysts. Mol Catal 485:110821. https://doi.org/10.1016/j.mcat.2020.110821
17. Chen H, Goodarzi F, Mu Y et al (2020) Effect of metal dispersion and support structure of Ni/silicalite-1 catalysts on non-thermal plasma (NTP) activated CO_2 hydrogenation. Appl Catal B Environ 272:119013. https://doi.org/10.1016/j.apcatb.2020.119013
18. Chen H, Mu Y, Xu S et al (2020) Recent advances in non-thermal plasma (NTP) catalysis towards C_1 chemistry. Chin J Chem Eng 28:2010–2021. https://doi.org/10.1016/j.cjche.2020.05.027
19. Stere CE, Adress W, Burch R et al (2014) Ambient temperature hydrocarbon selective catalytic reduction of NO_X using atmospheric pressure nonthermal plasma activation of a Ag/Al_2O_3 catalyst. ACS Catal 4:666–673. https://doi.org/10.1021/cs4009286
20. Wangkawong K, Phanichphant S, Inceesungvorn B et al (2020) Kinetics of water gas shift reaction on $Au/CeZrO_4$: a comparison between conventional heating and dielectric barrier discharge (DBD) plasma activation. Top Catal 63:363–369. https://doi.org/10.1007/s11244-020-01245-8
21. De Rosa F, Hardacre C, Graham WG et al (2021) Comparison between the thermal and plasma (NTP) assisted palladium catalyzed oxidation of CH_4 using AC or nanopulse power supply. Catal Today 384:177–186. https://doi.org/10.1016/j.cattod.2021.04.015
22. Baylet A, Marécot P, Duprez D et al (2012) Synergetic effect of plasma/catalysis hybrid system for CH_4 removal. Appl Catal B Environ 113–114:31–36. https://doi.org/10.1016/j.apcatb.2011.10.026
23. Lee H, Lee DH, Song YH et al (2015) Synergistic effect of non-thermal plasma-catalysis hybrid system on methane complete oxidation over Pd-based catalysts. Chem Eng J 259:761–770. https://doi.org/10.1016/j.cej.2014.07.128
24. Gibson EK, Stere CE, Curran-McAteer B et al (2017) Probing the role of a non-thermal plasma (NTP) in the hybrid NTP catalytic oxidation of methane. Angew Chem Int Edit 56:9351–9355. https://doi.org/10.1002/anie.201703550
25. Stere C, Chansai S, Gholami R et al (2020) A design of a fixed bed plasma DRIFTS cell for studying the NTP-assisted heterogeneously catalysed reactions. Catal Sci Technol 10:1458–1466. https://doi.org/10.1039/D0CY00036A
26 Nozaki T, Okazaki K (2013) Non-thermal plasma catalysis of methane: principles, energy efficiency, and applications. Catal Today 211:29–38. https://doi.org/10.1016/j.cattod.2013.04.002
27 Yao S, Chen Z, Weng S et al (2019) Mechanism of CO_2-formation promotion by Au in plasma-catalytic oxidation of CH_4 over $Au/\gamma\text{-}Al_2O_3$ at room temperature. J Hazard Mater 373:698–704. https://doi.org/10.1016/j.jhazmat.2019.04.003
28. Pham Huu T, Gil S, Da Costa P et al (2015) Plasma-catalytic hybrid reactor: application to methane removal. Catal Today 257:86–92. https://doi.org/10.1016/j.cattod.2015.03.001
29. Kim S-S, Kwon B, Kim J (2007) Plasma catalytic methane conversion over sol–gel derived Ru/TiO_2 catalyst in a dielectric-barrier discharge reactor. Catal Commun 8:2204–2207. https://doi.org/10.1016/j.catcom.2007.04.029
30. Kiani D, Sourav S, Tang Y et al (2021) Methane activation by ZSM-5-supported transition metal centers. Chem Soc Rev. https://doi.org/10.1039/D0CS01016B
31. Tang P, Zhu Q, Wu Z, Ma D (2014) Methane activation: the past and future. Energy Environ Sci 7:2580–2591. https://doi.org/10.1039/C4EE00604F
32. Horn R, Schlögl R (2015) Methane activation by heterogeneous catalysis. Catal Lett 145:23–39. https://doi.org/10.1007/s10562-014-1417-z
33. Hu X, Liu Y, Dou L et al (2022) Plasma enhanced anti-coking performance of Pd/CeO_2 catalysts for the conversion of methane. Sustain Energy Fuels 6:98–109. https://doi.org/10.1039/D1SE01441B
34 Smith JM, Van Ness HC, Abbott MM (2001) Introduction to chemical engineering thermodynamics, Sixth. McGraw-Hill, New York
35. Liu HF, Liu RS, Liew KY et al (1984) Partial oxidation of methane by nitrous oxide over molybdenum on silica. J Am Chem Soc 106:4117–4121. https://doi.org/10.1021/ja00327a009
36 Louis C, Tatibouët J-M, Che M (1988) Catalytic properties of silica-supported molybdenum catalysts in methanol oxidation: the influence of molybdenum dispersion. J Catal 109:354–366. https://doi.org/10.1016/0021-9517(88)90218-7

37. Chen Y, Zhang X, Wang X et al (2021) Insights into the structure-activity relationship in aerobic alcohol oxidation over a metal–organic-framework-supported molybdenum(VI) catalyst. J Am Chem Soc 143:4302–4310. https://doi.org/10.1021/jacs.0c12963
38. Kurlov A, Deeva EB, Abdala PM et al (2020) Exploiting two-dimensional morphology of molybdenum oxycarbide to enable efficient catalytic dry reforming of methane. Nat Commun 11:4920. https://doi.org/10.1038/s41467-020-18721-0
39. Suzuki K, Hayakawa T, Shimizu M, Takehira K (1994) Partial oxidation of methane over silica supported molybdenum oxide catalysts. Catal Lett 30:159–169. https://doi.org/10.1007/BF00813682
40. Xiao T, Hanif A, York APE et al (2002) Study on the mechanism of partial oxidation of methane to synthesis gas over molybdenum carbide catalyst. Phys Chem Chem Phys 4:4549–4554. https://doi.org/10.1039/B204347E
41 Gao Y, Dou L, Zhang S et al (2021) Coupling bimetallic Ni-Fe catalysts and nanosecond pulsed plasma for synergistic low-temperature CO_2 methanation. Chem Eng J 420:127693. https://doi.org/10.1016/j.cej.2020.127693
42. Gholami R, Smith KJ (2015) Activity of PdO/SiO2 catalysts for CH_4 oxidation following thermal treatments. Appl Catal B Environ 168–169:156–163. https://doi.org/10.1016/j.apcatb.2014.12.037
43. Danielis M, Betancourt LE, Orozco I et al (2021) Methane oxidation activity and nanoscale characterization of Pd/CeO_2 catalysts prepared by dry milling Pd acetate and ceria. Appl Catal B Environ 282:119567. https://doi.org/10.1016/j.apcatb.2020.119567
44. Molteni M, Donazzi A (2020) Model analysis of atmospheric non-thermal plasma for methane abatement in a gas phase dielectric barrier discharge reactor. Chem Eng Sci 212:115340. https://doi.org/10.1016/j.ces.2019.115340
45. Phan DQ, Kureti S (2017) CO oxidation on Pd/Al_2O_3 catalysts under stoichiometric conditions. Top Catal 60:260–265. https://doi.org/10.1007/s11244-016-0608-9
46. Xu W, Zhan Z, Di L, Zhang X (2015) Enhanced activity for CO oxidation over Pd/Al_2O_3 catalysts prepared by atmospheric-pressure cold plasma. Catal Today 256:148–152. https://doi.org/10.1016/j.cattod.2015.01.017
47. Taheraslani M, Gardeniers H (2020) Coupling of CH_4 to C_2 hydrocarbons in a packed bed DBD plasma reactor: the effect of dielectric constant and porosity of the packing. Energies 13:468. https://doi.org/10.3390/en13020468
48. Goujard V, Tatibouët J-M, Batiot-Dupeyrat C (2011) Carbon dioxide reforming of methane using a dielectric barrier discharge reactor: effect of helium dilution and kinetic model. Plasma Chem Plasma Process 31:315–325. https://doi.org/10.1007/s11090-010-9283-y
49. Jo S, Hoon Lee D, Seok Kang W, Song Y-H (2013) Methane activation using noble gases in a dielectric barrier discharge reactor. Phys Plasmas 20:083509. https://doi.org/10.1063/1.4818795
50. Wang W, Snoeckx R, Zhang X et al (2018) Modeling plasma-based CO_2 and CH_4 conversion in mixtures with N_2, O_2, and H_2O: the bigger plasma chemistry picture. J Phys Chem C 122:8704–8723. https://doi.org/10.1021/acs.jpcc.7b10619
51. Wu J, Xia Q, Wang H, Li Z (2014) Catalytic performance of plasma catalysis system with nickel oxide catalysts on different supports for toluene removal: effect of water vapor. Appl Catal B Environ 156–157:265–272. https://doi.org/10.1016/j.apcatb.2014.03.017
52. Falkenstein Z, Coogan JJ (1997) Microdischarge behaviour in the silent discharge of nitrogen–oxygen and water–air mixtures. J Phys D Appl Phys 30:817–825. https://doi.org/10.1088/0022-3727/30/5/015
53. Zhang J, Liu Y, Yao X et al (2020) Enhanced moisture resistance of Cu/Ce catalysts for CO oxidation via plasma−catalyst interactions. Chemosphere 261:127739. https://doi.org/10.1016/j.chemosphere.2020.127739
54. Wang Z, Kuang H, Zhang J et al (2019) Nitrogen oxide removal by non-thermal plasma for marine diesel engines. RSC Adv 9:5402–5416. https://doi.org/10.1039/C8RA09217F
55. Snoeckx R, Heijkers S, Van Wesenbeeck K et al (2016) CO_2 conversion in a dielectric barrier discharge plasma: N_2 in the mix as a helping hand or problematic impurity? Energy Environ Sci 9:999–1011. https://doi.org/10.1039/C5EE03304G
56. Pavlovich MJ, Ono T, Galleher C et al (2014) Air spark-like plasma source for antimicrobial NO_X generation. J Phys D Appl Phys 47:505202. https://doi.org/10.1088/0022-3727/47/50/505202
57. Nova I, Tronconi E (2014) Urea-SCR technology for deNO_X after treatment of diesel exhausts, 1st edn. Springer, New York
58. Villamaina R, Nova I, Tronconi E et al (2019) Effect of the NH_4NO_3 addition on the Low-T NH_3-SCR performances of individual and combined Fe- and Cu-zeolite catalysts. Emiss Control Sci Technol 5:290–296. https://doi.org/10.1007/s40825-019-00140-3
59. Tokunaga O, Suzuki N (1984) Radiation chemical reactions in NO_X and SO_2 removals from flue gas. Radiat Phys Chem 24:145–165. https://doi.org/10.1016/0146-5724(84)90013-X

60. Zhao W, Liu Y, Wei H et al (2019) NO removal by plasma-enhanced NH_3-SCR using methane as an assistant reduction agent at low temperature. Appl Sci 9:2751. https://doi.org/10.3390/app9132751
61. Bogaerts A, Tu X, Whitehead JC et al (2020) The 2020 plasma catalysis roadmap. J Phys D Appl Phys 53:443001. https://doi.org/10.1088/1361-6463/ab9048